Catalysis in Solid Oxide Fuel Cells

R.J. Gorte and J.M. Vohs

Department of Chemical and Biomolecular Engineering, University of Pennsylvania, Philadelphia, Pennsylvania 19104; email: gorte@seas.upenn.edu, vohs@seas.upenn.edu

Annu. Rev. Chem. Biomol. Eng. 2011. 2:9–30

First published online as a Review in Advance on December 3, 2010

The *Annual Review of Chemical and Biomolecular Engineering* is online at chembioeng.annualreviews.org

This article's doi:
10.1146/annurev-chembioeng-061010-114148

1947-5438/11/0715-0009$20.00

Keywords

electrolyzers, cathodes, anodes, electrode impedance, electrode stability

Abstract

Solid oxide fuel cells (SOFCs) and solid oxide electrolyzers (SOEs) hold much promise as highly efficient devices for the direct interconversion of chemical and electrical energy. Commercial application of these devices, however, requires further improvements in their performance and stability. Because the performance of SOFC and SOE electrodes depends on their microstructures, electronic and ionic conductivities, and chemical reactivities, the needed improvements require the expertise of various disciplines, with catalytic science playing an important role. Highly active and thermally stable catalysts are required to limit the internal losses in the devices, increase the range of fuels they can use, and decrease the temperatures at which they operate. In this article we review some of the most important recent advances in catalysis for SOFC and SOE electrodes and highlight additional improvements that are needed.

INTRODUCTION

Solid oxide fuel cells (SOFCs) and solid oxide electrolyzers (SOEs) seem destined to find widespread future application for conversion between chemical and electrical energy because of their intrinsic high efficiencies. As with all fuel cells and electrolyzers, the conversion between fuel and power occurs electrochemically, without moving parts. The same device can be used to generate power or chemicals simply by reversing the direction of the current. Because SOFCs and SOEs operate at high temperatures, 773 to 1,273 K, electrode losses tend to be much smaller than those obtained in their lower-temperature counterparts. Furthermore, SOFCs and SOEs based on electrolytes that are oxygen-ion conductors also offer much greater fuel flexibility than low-temperature devices based on proton-conducting electrolytes. In principle, SOFCs can generate electrical power using any combustible fuel (1), and SOEs are capable of reducing CO_2 to CO almost as easily as H_2O to H_2 (2, 3).

Many good reviews describe each component of an SOFC, including the electrolyte (4, 5), the anode (6, 7), and the cathode (8). We do not attempt to duplicate that literature but summarize some of the key operating principles of this device. In this paper we address catalytic issues associated with solid oxide electrodes, including what is known and where more progress is required. Although reforming catalysis in SOFCs is an important topic (9), we consider this application only briefly. The primary focus here is on the electrode catalysis required for high-performance electrodes. Because yttria-stabilized zirconia (YSZ) and scandia-doped zirconia (SDZ) are the standard electrolytes used in SOFCs, the discussion focuses on systems using these electrolytes.

SOLID OXIDE FUEL CELL AND SOLID OXIDE ELECTROLYZER OPERATING PRINCIPLES

Equilibrium Thermodynamics

The operating principles of an SOFC are illustrated in **Figure 1** (reverse the direction of the arrows for operation in electrolysis mode). At the cathode, O_2 from air is catalytically reduced to oxygen anions, O^{2-}, via the half-cell reaction, Equation 1:

$$\tfrac{1}{2}O_2 + 2e^- \rightarrow O^{2-}. \qquad 1.$$

The oxygen ions are then transported through the electrolyte membrane to the anode, where they react with the fuel, H_2 in this example, to produce H_2O and electrons according to the other half-cell reaction, Equation 2:

$$O^{2-} + H_2 \rightarrow H_2O + 2e^-. \qquad 2.$$

The electrons produced at the anode are at a higher potential than those consumed at the cathode and therefore can do work in an external circuit. In an ideal, reversible fuel cell, the work the electrons are capable of doing is equal to the Gibbs free energy of the oxidation reaction, ΔG_{rxn}, which is in turn related to the O_2 fugacities (or partial pressures) at the cathode and anode by Equation 3,

$$\Delta G_{rxn} = RT \ \ln[P(O_{2,anode})/P(O_{2,cathode})]. \qquad 3.$$

$P(O_{2,anode})$ is the fugacity established by equilibrium with the H_2 and H_2O present in the anode compartment. Upon substituting the appropriate equilibrium expression for $P(O_{2,anode})$ and

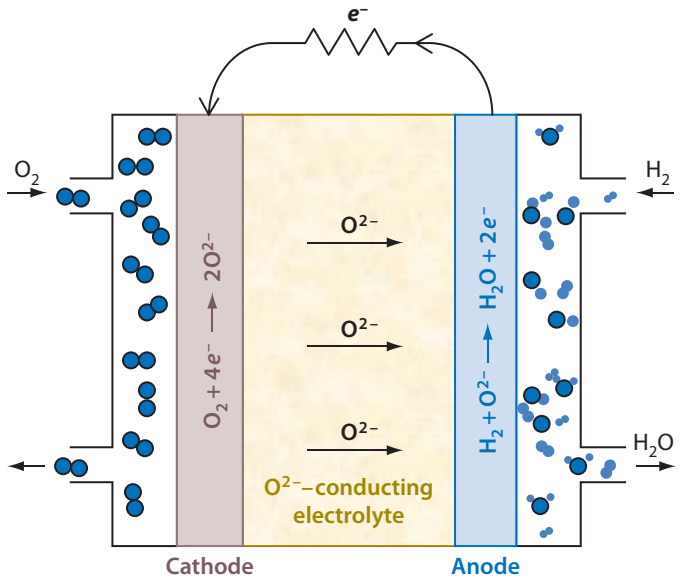

Figure 1

Schematic diagram of a solid oxide fuel cell (SOFC) showing the electrolyte, the electrodes and electrode reactions, and the direction of electron and ion flow. Reverse the direction of the arrows for operation in electrolysis mode.

converting to electrical units, Equation 3 becomes the Nernst equation, Equation 4:

$$V_{\text{Nernst}} = V^0 + \frac{RT}{nF} \ln \left(\frac{P_{\text{H}_2,\text{anode}} \cdot P_{\text{O}_2,\text{cathode}}^{\frac{1}{2}}}{\text{P}_{\text{H}_2\text{O},\text{anode}}} \right). \quad 4.$$

Here, V^0 is the equilibrium potential at standard conditions, n is the number of electrons taking part in each half-cell reaction, and F is Faraday's constant, the number of coulombs in a mole of electrons.

These thermodynamic relations apply equally well to SOEs; the only difference is the direction of the arrows in the half-cell reactions. Also, because a cathode is the electrode where reduction takes place and an anode is where oxidation takes place, in an SOE the electrode exposed to O_2 becomes the anode and the electrode exposed to the fuel becomes the cathode. Therefore, when discussing SOFCs and SOEs together, it is sometimes convenient to refer to the electrodes as the "air" and "fuel" electrodes.

Energy Losses in Solid Oxide Fuel Cells and Solid Oxide Electrolyzers

For operation with H_2, the cell potential at open circuit in an SOFC/SOE with a YSZ electrolyte is usually very close to the Nernst potential predicted from Equation 4. This is not the case for some electrolytes, such as doped ceria (cerium dioxide), which have mixed ionic and electronic conductivity (MIEC), which causes the open-circuit voltage (OCV) to be lower. When current is flowing through the cell, however, irreversible processes in the electrolyte and electrodes cause the cell potential to be lower; the lost energy generates heat. The losses in the electrolyte are simple to describe. Because every material has an intrinsic conductivity, the area-specific resistance, R_E, can be calculated from the conductivity and the thickness of the electrolyte (5). The potential energy

loss in the electrolyte for a current density, i, is equal to $i \cdot R_E$, which can be kept small through the choice of temperature and by using thin electrolyte layers.

Because the electrodes must be made from materials that have good electronic conductivity, $i \cdot R$ drops in the electrodes are typically small; however, mass transport of the gaseous reactants to the electrolyte interface and slow reaction kinetics for the electrode reactions can lead to potential drops, referred to as the electrode overpotentials, η_{anode} and $\eta_{cathode}$. As discussed below, these are expected to depend strongly on the current density in ways that may be complex. Therefore, the cell potential will vary with current density according to Equation 5,

$$V = V_{Nernst} - (iR_E + \eta_{anode} + \eta_{cathode}). \quad 5.$$

Mass transport losses, also known as concentration overpotentials, occur when diffusion of the reacting species from the electrode compartment to the electrolyte interface causes the concentration of the reacting species at the electrolyte interface to be lower than that used in calculating the Nernst Potential. This is a problem primarily at high current densities and in dilute reactant streams. For example, when operating a cell on H_2 at high fuel utilization, the H_2 becomes diluted in steam. Because the diffusive flux to the electrode is proportional to $dP(H_2)/dx$ and must match the current density, i, the value of $P(H_{2,anode})/P(H_2O_{anode})$ at the electrolyte interface can also differ significantly from its value in the anode compartment. Closed-form expressions for the concentration overpotentials can be obtained in terms of the effective diffusivities and the partial pressures of the reacting gases (10).

Losses due to the electrochemical reactions are important in determining the performance of the cell but are the most difficult to describe. Because reducing these losses is the primary goal of electrode catalysis, we consider the physical situation in some detail in the next sections. The reader should recognize that our understanding of electrochemical processes in solid oxide electrodes is incomplete and that disagreements still exist among researchers in this area.

Three-Phase Boundary

It is apparent from the electrode reactions in Equations 1 and 2 that three distinct species, a gas-phase molecule, electrons, and oxygen ions, must be present simultaneously for the reactions to take place. If the electrode material has only electronic conductivity and the electrolyte has only ionic conductivity, these three species can come together only at the three-phase boundary (TPB) line, the line of contact for the electrode, the electrolyte, and the gas phase (11). Many materials used in SOFC electrodes are MIEC, and for these systems the TPB line will have a finite width. This is particularly true for the best air electrodes, such as Sr-doped $LaCo_{0.2}Fe_{0.8}O_3$ (LSCF), a good electronic conductor that also has ionic conductivity approaching that of YSZ (12). Because the electrochemically active region of good electrodes typically extends at least several micrometers from the electrolyte interface (11, 13), it is reasonable to assume that the TPB is tens of nanometers wide in some cases.

The best electrodes, for both fuel and air sides, are composites of the electronic conductor and the electrolyte. The use of composites provides several important advantages that are not the focus of this review, including prevention of the sintering of metal electrodes, improved matching of the coefficient of thermal expansion (CTE) with the electrolyte, and increased mechanical stability (14). In terms of their catalytic properties, it is important that composites also have a much longer TPB line than electrodes made without the electrolyte material and, therefore, more active sites (11). As shown in **Figure 2**, the presence of the electrolyte within the electrode provides ion-conducting channels that allow O^{2-} ions to migrate into the electrode. **Figure 2** also demonstrates that each of the three phases within the composite must percolate the structure

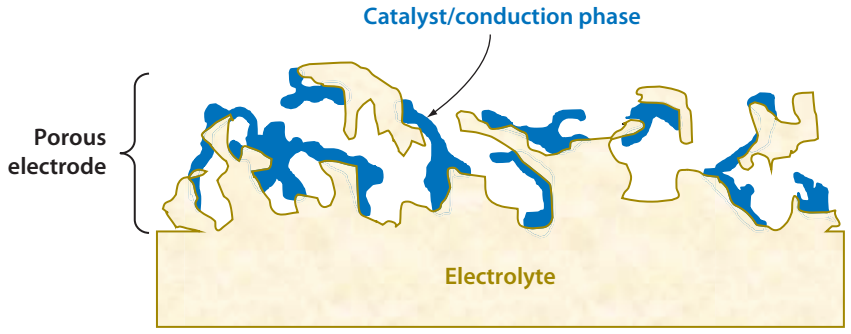

Figure 2

Schematic diagram of a solid oxide fuel cell/solid oxide electrolyzer (SOFC/SOE) electrode. The electrochemical reactions can occur only at those sites where the gas phase, the electronic conductor, and the electrolyte—the three-phase-boundary (TPB) sites—come in simultaneous contact. Electrolyte material that is not in contact with the electrolyte itself cannot contribute.

(15). For example, if the component that provides electronic conductivity within the composite is not in electrical contact with the external circuit, it cannot provide electrons for the half-cell reactions. Because the percolation threshold in random composites is approximately 30 vol%, obtaining the necessary composition and structure for optimal electrochemical performance is challenging.

To optimize mechanical properties and performance, the best electrodes are split into a thin functional layer near the electrolyte and a thicker current-collection layer on top of the functional layer (16, 17). Because electrochemical reactions do not occur in the current-collection layer, it is generally engineered to have a high porosity to facilitate the diffusion of reactants and a high conductivity to decrease ohmic losses. The functional layer is typically 5–10 μm thick and designed to optimize the TPB length. It needs only enough conductivity and porosity to minimize potential drops and concentration differences across this thickness.

Electrochemical Reactions

The kinetics of electrochemical reactions is usually modeled using the Butler-Volmer equation, Equation 6:

$$i = i^0 \left[\exp\left(\frac{\beta z F \eta^{act}}{RT} \right) - \exp\left(\frac{(1-\beta) z F \eta^{act}}{RT} \right) \right]. \qquad 6.$$

In this equation, i is the current density in the cell, β is a dimensionless constant (less than one) known as the transfer coefficient, z is the number of electrons in the reaction, i^0 is the exchange current density, and η^{act} is the electrode overpotential associated with the electrochemical reaction. The equation was originally derived to describe reactions that take place at metal surfaces in solution, where most of the change in potential occurs across a double layer that is approximately 1–2 nm thick (18). For reactions in which at least one species is charged, the field gradients associated with the change in potential over this short distance are large enough to alter the reaction coordinate that describes the rate constant, effectively lowering the energy barrier to the transition state, as shown diagrammatically in **Figure 3**. Although Equation 6 does not provide a simple expression for η^{act} as a function of current density, it is apparent that the relationship is highly nonlinear, so that the slope of a *V-i* polarization curve for a system in which the reaction kinetics adheres to this equation should be highly nonlinear.

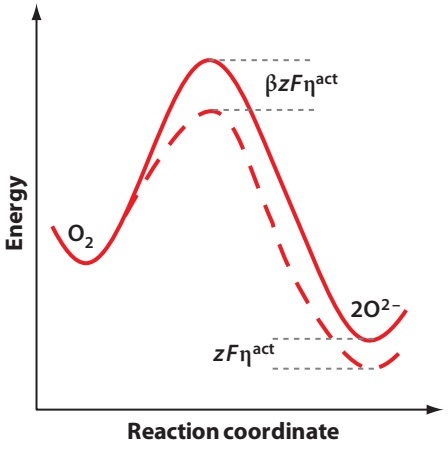

Figure 3

Reaction coordinate diagram for an electrode reaction that adheres to the Butler-Volmer equation. The solid and dashed lines correspond to open circuit and closed circuit conditions, respectively. At closed circuit the potential difference between the electrode and electrolyte (i.e., the electrode overpotential) modifies the reaction coordinate.

Butler-Volmer behavior is commonly observed in proton exchange membrane fuel cells (PEM-FCs) in which the catalytic metals near the electrolyte interface are effectively immersed in water to facilitate transfer of ions into the electrolyte. The situation for solid oxide electrodes is far less clear, however. Although a potential difference equal to the electrode overpotential must still exist at the electrode-electrolyte interface, the length scale over which this occurs is likely to be on the order of 1 μm (10), because there is no double layer analogous to that for an electrode immersed in a solution phase. This implies that field gradients in the solid oxide electrode will be relatively small. Because distances along the reaction coordinate should be similar to bond distances, ~0.1 nm, field gradients less than 0.01 V nm^{-1} would not be expected to significantly affect the barrier height for most reactions.

The literature contains many examples in which the *V-i* polarization curves for SOFCs are linear, implying that the electrode impedance is independent of current density, and the *V-i* curve has identical slopes under both cathodic and anodic polarization (2, 19, 20). For example, **Figure 4** shows the *V-i* polarization and impedance plots for a cell operating in a 50% CO–50% CO_2 mixture and under both fuel-cell (positive currents) and electrolyzer (negative currents) conditions. Details on the electrode compositions are given elsewhere (2, 21). The main point here is that there is no evidence for nonlinear behavior, even for an electrode operating at moderate temperatures in CO-CO_2 mixtures, a mixture that should be more difficult to activate than the more usual H_2-H_2O situation. The *V-i* plot in **Figure 4*a*** is clearly linear; furthermore, the impedance spectrum in **Figure 4*b*** shows that this example is not a simple case in which performance is limited by the electrolyte, with negligible electrode losses. Because of the different timescales for electrode and electrolyte processes, the real-axis intercept at high frequencies (0.42 Ω cm^2) can be identified with R_E, whereas the width of the arc (~0.30 Ω cm^2) in the impedance curve is equal to the sum of the impedances of the two electrodes at that current density (22). In agreement with the linear *V-i* relationship, the impedance spectra indicate that the electrode impedances are invariant under both fuel-cell and electrolyzer conditions.

Many processes could be rate limiting and give rise to a current-independent electrode impedance. With air electrodes, for example, a model that assumes that electrode performance

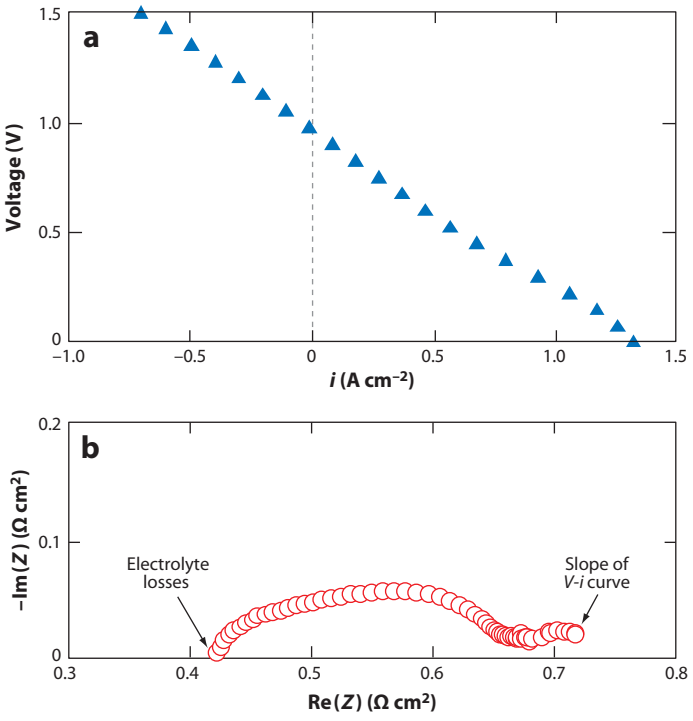

Figure 4

(*a*) *V-i* polarization and (*b*) impedance plot for a cell operating under both fuel-cell (positive currents) and electrolyzer (negative currents) conditions. The fuel electrode is operating in a 50% CO–50% CO_2 mixture.

is limited by O^{2-} diffusion through a dense layer of an MIEC conductor gives rise to constant impedances (23), as does a model that assumes O_2 adsorption is rate limiting (24). Nonlinear *V-i* curves may also result from processes other than Butler-Volmer electrode kinetics. For example, with air electrodes made from Sr-doped $LaMnO_3$ (LSM), nonlinear *V-i* behavior is at least sometimes associated with processes that are irreversible on a timescale less than several hours (25). This suggests that the nonlinearity is due to structural or compositional changes at the LSM-electrolyte interface (26–28), because perturbation of the reaction coordinate by field gradients would be instantly reversible.

In any case, when the impedances of the two electrodes, $R_{cathode}$ and R_{anode}, are independent of current density, Equation 5 becomes:

$$V = V_{Nernst} - i(R_E + R_{anode} + R_{cathode}). \quad 7.$$

Because a reasonable goal is for the total area-specific resistance (ASR, equal to $R_E + R_{cathode} + R_{anode}$) of the cell to be less than ~0.3 Ω cm^2 (5), for an ASR corresponding to a maximum power density of 1 W cm^{-2} in an SOFC, each of the components should have an impedance of approximately 0.1 Ω cm^2 or less.

Non-Faradaic, Electrochemical Modification of Chemical Activity

Related to the effect of fields on electrochemical reactions in solid oxide electrodes is an interesting phenomenon referred to as non-Faradaic, electrochemical modification of chemical activity

(NEMCA) (29, 30). In NECMA, an increase in catalytic activity, many orders of magnitude in some cases, and selectivity occurs for catalytic reactions on electrodes composed of a metal supported on an oxygen-ion-conducting electrolyte, upon application of a potential. The initial hypothesis for NEMCA was that the applied potential caused a change in the work function of the metal, possibly through the spillover of oxygen ions from the electrolyte, and this change in electronic properties affected the intrinsic rates of adsorption and surface reactions (30). An alternative explanation for the NEMCA effect for catalysts involving oxygen-ion conductors is that the O^{2-} ions that are pumped onto the supported metal catalyst via application of a potential alter the concentrations of adsorbed reactants and intermediates (31, 32).

To illustrate this second concept, consider ethylene oxidation over Pt supported on zirconia (zirconium dioxide), a reaction that has been reported to exhibit a large NEMCA effect (33). Single crystal studies show that the adsorption rates for both ethylene and O_2 on clean Pt surfaces are quite high (sticking coefficients near unity), and reaction between the coadsorbed species formed from ethylene and oxygen occurs rapidly at temperatures well below those for which NEMCA is reported for this system (34). Under normal, steady-state reaction conditions at atmospheric pressure, however, the ethylene oxidation rate is much lower than that predicted by the kinetics of the elementary steps measured in vacuum. This is likely because under realistic reaction conditions the Pt surface becomes covered with carbonaceous residues that block sites for O_2 adsorption. In this case, application of a potential to a Pt/ZrO_2 electrode would result in the pumping of O^{2-} ions to the surface, causing the removal of carbon and thereby exposing the active Pt sites (31). This process would have a nonlinear effect on the reaction rate because the carbon buildup occurs relatively slowly. This effect is also similar to that observed for some reactions over noble metals on reducible oxide supports such as CO oxidation on ceria-supported Pt (35). For example, in excess CO, the reaction rate is limited by O_2 adsorption on a CO-saturated surface. Large rate enhancements are observed with Pt-ceria catalysts owing to removal of some of the CO on the Pt via reaction with oxygen supplied by the ceria support.

Although we do not believe that NEMCA is an electronic effect, the ability to tailor the concentrations of surface species can still be important as a way to use catalysts under conditions that would not be possible under ordinary reaction conditions. Although the NEMCA effect has not been documented for working electrodes in SOFC and SOE devices, it is possible that it plays a role in determining the overall kinetics of the electrode reactions.

ROLE OF CATALYSIS IN FUEL ELECTRODES

Nickel-Based Electrodes

The standard material in SOFC anodes and SOE cathodes based on YSZ electrolytes is a ceramic-metallic (cermet) composite of Ni and YSZ (14), with Ni providing both electronic conductivity and catalytic activity in this application. In an anode-supported SOFC, the Ni also provides mechanical strength to the cell, so that one can use very thin (<10 μm) electrolytes (36). Because Ni is an outstanding catalyst for methane-steam reforming, it is possible to cofeed steam and methane to the cell, using the electrode itself as the reforming catalyst (37).

Separating the effects of catalytic activity and conductivity in Ni cermets is not easy to do in most cases. To understand the main characteristics of Ni-YSZ electrodes, it is useful to consider how the best electrodes are made. For an anode-supported SOFC with YSZ electrolytes, a mixture of NiO and YSZ powders is typically sintered together with a thin layer of YSZ at temperatures between 1,573 and 1,773 K (17, 36). After applying the cathode material to the opposite side of the YSZ electrolyte, the NiO is reduced to metallic Ni by exposure to H_2 at the fuel-cell operating

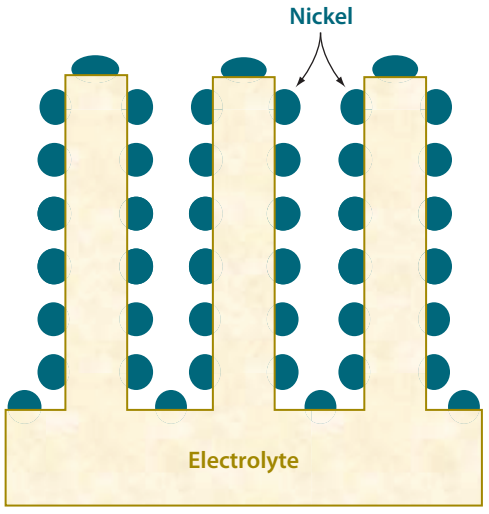

Figure 5

Idealized structure of a solid oxide fuel cell/solid oxide electrolyzer (SOFC/SOE) electrode in the first 10 μm near the electrolyte interface. The nickel phase is shown as particles on the electrolyte fingers that extend into the electrode, but must be connected for electrons produced by the electrochemical reaction to flow to the external circuit.

temperature. The reduction in volume in going from NiO to Ni creates porosity in the anode layer. The Ni must be present in quantities greater than approximately 30 vol% to provide electrical conductivity (15). Because the composites have been fired to extremely high temperatures, the typical grain size in the electrode approaches 1 μm. The surface area for this type of electrode is likely on the order of 1 $m^2\ g^{-1}$ (26, 27).

The cosintering of the NiO-YSZ with the YSZ in electrode-supported cells is a key factor in establishing an electrode structure capable of high performance. Electrolyte-supported cells, which are often prepared by applying NiO-YSZ mixtures onto a presintered, dense YSZ electrolyte layer, always perform much worse, even when the electrode compositions are the same. Performance characteristics for electrolyte-supported cells are usually reported at higher temperatures, above 1,173 K (38), whereas comparable power densities in anode-supported cells can be achieved at 973 K. Because the electrolyte losses are negligible at 1,173 K for a typical YSZ electrolyte thickness of 150 μm (5) and the cathodes are the same in both cases, the anodes in the electrolyte-supported cells must be greatly inferior. Cosintering of the NiO-YSZ composite with the YSZ in the anode-supported cells causes both layers to shrink simultaneously, and this appears to provide a much better interface between the electrode and the electrolyte [i.e., there are good YSZ channels for ion conduction from the electrolyte into the electrode, as shown schematically in **Figure 5** (11)].

Ni composites are widely used because they are relatively easy to fabricate and work well. The impedance of Ni-YSZ can be low for operation in H_2 or synthesis gas (syngas, a mixture of H_2 and CO). Although it is difficult to separate cathode impedances from anode impedances in anode-supported cells (22), SOFCs with Ni-YSZ anodes have achieved greater than 0.8 W cm^{-2} at 923 K under conditions for which the cathode likely limits performance (39). Although there are long-term stability issues for Ni-YSZ anodes, these cells have been operated successfully for months with negligible changes in performance.

There are problems, however, with Ni-based anodes that could be solved by using alternative materials. One of the biggest drawbacks of Ni is that it catalyzes the formation of carbon fibers

when exposed to hydrocarbons and even CO at the elevated temperatures used in SOFCs (1). The mechanism for this involves deposition of carbon on the Ni surface, dissolution of the carbon into the bulk of the Ni, and precipitation of the carbon in the form of graphite fibers at some nucleation point on the Ni. In addition to causing deactivation of the electrode by covering the Ni surface, the formation of fibers can lead to loss of the Ni by a corrosion process known as metal dusting (40) and to fracture of the cells due to stresses caused by the growing fibers (41). These problems effectively prevent the direct utilization of hydrocarbons in SOFCs (42) and limit the conditions that can be used for CO_2 electrolysis in SOEs (43).

Other major problems with Ni-YSZ anodes are redox instability (44) and intolerance to low levels of sulfur (45, 46). The redox instability is associated with re-expansion of Ni upon formation of NiO, which can lead to cell fracture. Reoxidation can occur near seals in the event of a leak and during shutdown procedures because Ni will oxidize at high H_2O:H_2 ratios and lower temperatures. Even though the H_2S:H_2 ratios required to form bulk Ni sulfides are relatively high, studies have shown that sulfur concentrations as low as 1 ppm cause significant degradation in the performance of Ni-YSZ anodes (45, 46), apparently owing to surface sulfides on Ni. Progress on the development of electrodes with improved sulfur tolerance has been reviewed elsewhere (47).

Modification of Nickel Electrodes

Ni-based anodes could be used for direct utilization of hydrocarbons if it were not for the problems of carbon formation and poor sulfur tolerance. Therefore, it is not surprising that significant effort has gone into modifying Ni cermets to take advantage of their good properties and ameliorate their problems. One approach is to physically protect the Ni from conditions under which it is not stable by placing either a carbon-tolerant catalyst or a diffusion barrier on the external surface of the electrode. For example, Barnett and coworkers (48) used a thin outer layer containing a Ru/ceria catalyst to reform higher-molecular-weight hydrocarbons into syngas before they came into contact with the Ni. In another study, this same group applied a diffusion barrier consisting of $La_{0.2}Sr_{0.8}TiO_3$ (LST, an electronically conductive oxide) onto the external surface of the electrode (49). The LST barrier appeared to help maintain a higher steam pressure in the vicinity of the Ni when current was being drawn. Because diffusion limitations are normally to be avoided in solid oxide electrodes, it remains to be seen whether this approach is practical. In any case, these approaches do not involve modifications of the catalytic properties of the metal.

There have also been many attempts to modify the properties of the Ni itself so as to avoid carbon deposition. Here we focus on two examples. In the first, Ni was alloyed with Cu, a metal that does not catalyze the formation of carbon fibers (50, 51). Because CuO melts at temperatures below that necessary for sintering YSZ electrolytes and also forms a solution with YSZ, alternative methods were needed to prepare the Cu-Ni alloy electrodes. In one study, the Cu-Ni alloy electrodes were formed using an infiltration procedure described later in this review (50). In a second study, Cu was electroplated onto the surface of a Ni-YSZ composite (51). Carbon formation due to exposure of the electrode to methane at high temperatures was suppressed in both studies but at the expense of electrochemical performance.

A second and more interesting modifier for Ni is Sn (52–55). Unlike Cu, Sn does not form a bulk alloy with Ni. It does, however, form a surface alloy that apparently does not significantly affect the electrochemical and conduction properties of the Ni. In one study, Ni-based electrodes were tested in methane and isooctane, before and after the addition of 0.5 to 1.0 wt% Sn, and the Sn greatly decreased the carbon deposit–forming activity of the electrodes (52).

Other modifications to the catalytic properties of Ni-cermet electrodes have been aimed at improving their sulfur tolerance (45, 56). The most interesting results in this area were reported

by Kurokawa et al. (45), who used infiltrated ceria nanoparticles to modify a conventional Ni-YSZ anode. These authors found that adding 40 ppm H_2S to the anode H_2 feed stream of an unmodified SOFC caused the cell voltage to drop to zero within several minutes. After the addition of ceria nanoparticles, the addition of 40 ppm H_2S caused the cell voltage to drop from 0.78 to 0.6 V after several minutes, but then the performance was stable for the next 500 h. Switching the feed stream back to pure H_2 restored the initial performance of the cell.

Using Alternatives to Nickel in Solid Oxide Fuel Cell Anodes

Many electronically conductive materials have been tested as SOFC anodes; reviews of this work can be found elsewhere (7, 57, 58). The electrode-performance characteristics of most of these materials are poor compared with that of Ni, and they usually require much higher operating temperatures to achieve reasonable impedances. A primary reason for this is that many of these alternatives are not good catalysts (59). Some of the poor performance is also due to the critical nature of the interfacial structure between the electrode and electrolyte for establishing good electrodes. Unfortunately, the cosintering process described for Ni-based, electrode-supported SOFCs does not work well for electrodes made from most other metals or conducting oxides. For example, oxides of Co form solutions with YSZ at the sintering temperatures required for making a dense YSZ electrolyte, and different, more complex methods must be used to make Co-YSZ composites that produce electrodes that exhibit low impedances (60).

Recently, an alternative method has been developed for establishing a good electrode-electrolyte interface with materials other than Ni (61–64). The method, shown schematically in **Figure 6**, involves preparing a bilayer YSZ structure containing one porous and one dense layer, and then infiltrating the porous layer with the active component. The porous and dense layers can be calcined together to produce high connectivity between the electrolyte and electrode prior to addition of the active component, thereby eliminating the need to heat the active component to the YSZ sintering temperature. For catalytic studies, the infiltration procedure also provides an ideal test bed in that a comparison can be made between various materials while maintaining the structure of the YSZ phase fixed.

There are many ways to prepare the porous-dense YSZ structure. The method developed in our laboratory involves tape casting (61, 62). Two green tapes are prepared, one of which contains sacrificial pore formers, such as graphite powder. The tapes are then laminated and fired to temperatures sufficient to make the layer without pore formers dense but leave cavities where the pore formers had been in the other layer. Another approach involves leaching out the Ni in a Ni-based, electrode-supported cell with nitric acid (65). Although somewhat more complicated, this alternative procedure results in a YSZ structure that is similar to that found in electrode-supported cells.

Copper-Based Electrodes

The infiltration procedure was first used to produce SOFC anodes based on infiltration of Cu and ceria into porous YSZ (66). Electrodes of this design were shown to be highly resistant to fouling when used with hydrocarbon-based fuels and exhibit stable performance when running on methane and higher hydrocarbons, at least under some conditions (67, 68). The Cu in these electrodes primarily provided electronic conductivity; ceria was required as an oxidation catalyst. The evidence for this was as follows: First, when Cu alone was present in the electrode (no ceria), the electrode impedance was quite high, especially when the fuel was dry methane (67). Replacing Cu with Au, a metal that would be expected to exhibit poor catalytic activity, had essentially

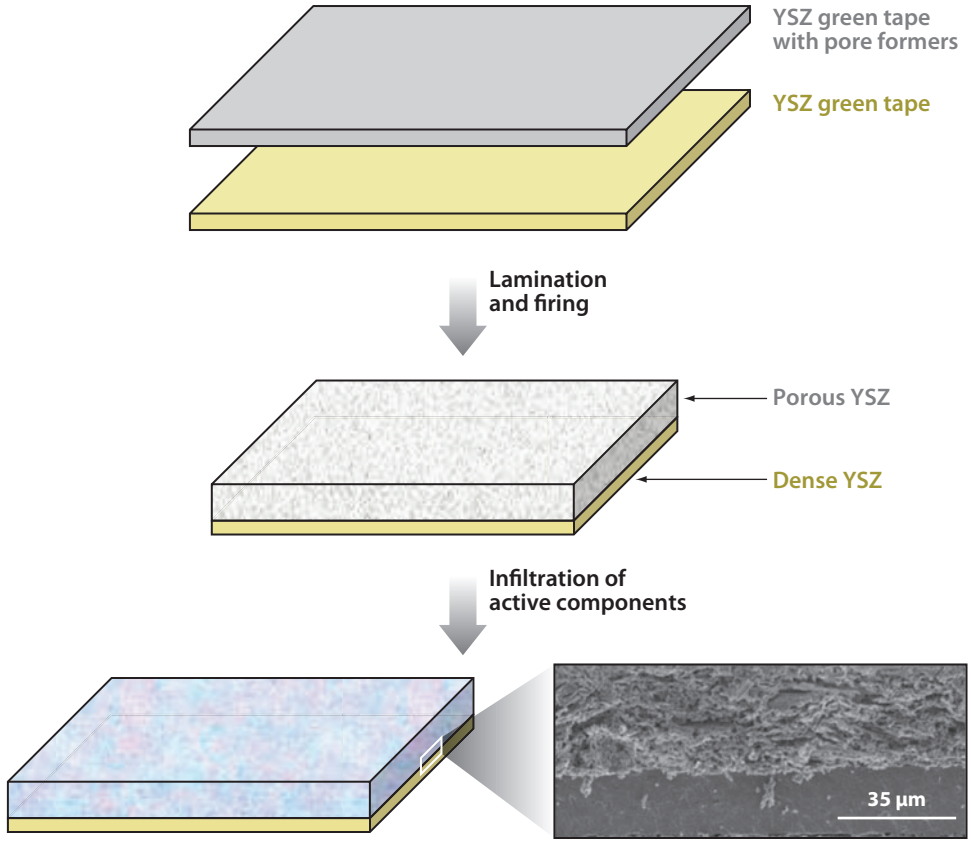

Figure 6

Roadmap for the synthesis of solid oxide fuel cell/solid oxide electrolyzer (SOFC/SOE) electrodes using porous-dense yttria-stabilized zirconia (YSZ) bilayers and infiltration of active components.

no effect (69). Reasonable electrode performance was obtained only after the addition of ceria. When other oxides were substituted for ceria, the electrode performance scaled with the catalytic activity of the oxide (70). Particularly noteworthy was the observation that when the catalyst was molybdena (molybdenum oxide), which selectively oxidizes hydrocarbons, and the fuel was propene, the anode reaction exhibited high selectivity for the production of acrolein, the selective oxidation product. These results all point toward a mechanism in which the oxide is reduced by the fuel and then reoxidized by the underlying YSZ electrolyte, with Cu removing the electrons required for transfer of oxygen from the YSZ (**Figure 7**). This work has been reviewed elsewhere (1).

One drawback of the Cu-based electrodes is that they have limited thermal stability (71). Heating cells to 1,173 K has been shown to cause sintering of the Cu and a consequent loss of connectivity that yields an increase in the ohmic resistance of the cells. Attempts have been made to stabilize the Cu by electrodeposition of a more refractory metal onto the Cu film; the most successful of these efforts used Co (72). Although Co can catalyze the formation of carbon fibers in a manner similar to that of Ni, minimization of surface energies causes Cu to migrate to the surface of the Cu-Co particles (73), resulting in electrodes with the carbon tolerance of Cu and the thermal stability of Co.

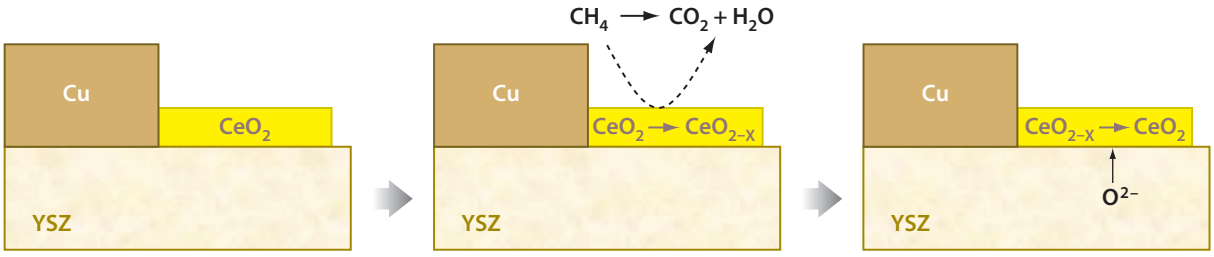

Figure 7

Proposed mechanism for the direct oxidation of a hydrocarbon on a fuel electrode composed of copper, yttria-stabilized zirconia (YSZ), and ceria.

Ceramic Solid Oxide Fuel Cell Anodes

SOFC anodes based on ceramic conductors could have many important advantages (7), including stability against carbon-fiber formation when using hydrocarbon-based fuels and less sensitivity to oxidation and reduction cycles. For operation with hydrocarbon fuels, the ability to oxidize the anode is particularly useful, as periodic oxidation cycles will remove impurities brought in with the fuel or carbon deposits formed by gas-phase pyrolysis, should this be necessary. Because many ceramics have high melting temperatures, excellent thermal stability is also anticipated for electrodes based on conducting oxides. The two primary problems with oxide-based electrodes are that they often have insufficient electronic conductivity in the fuel-electrode environment and that they exhibit relatively poor catalytic activity for oxidation reactions. Other reviews describe approaches for dealing with the difficulties associated with low electronic conductivity (7, 57). The low catalytic activity of oxides compared with that of transition metals such as Pt and Ni for normal heterogeneous combustion reactions is of course well known.

We have studied the catalytic requirements for electrodes based on electronically conducting ceramics prepared using infiltration procedures, taking advantage of the flexibility for composition modification that this fabrication procedure provides (74, 75). For example, *V-i* polarization curves and impedance plots for otherwise identical SOFCs, with anodes consisting of infiltrated $La_{0.8}Sr_{0.2}Cr_{0.5}Mn_{0.5}O_3$ (LSCM) and various catalytic species in porous YSZ, are shown in **Figure 8** (75). The data are reported for operation at 973 K with humidified H_2 (3% H_2O) for cells that contained either no added catalyst, 5-wt% ceria, 0.5-wt% Pd, or both 5-wt% ceria and 0.5-wt% Pd. **Figure 8*a*** demonstrates that the maximum power density of the cell without any added catalyst was only 105 mW cm^{-2} and that the addition of 5-wt% ceria increased this to 300 mW cm^{-2}. The power density increased still further after the addition of 0.5-wt% Pd alone or addition of 0.5-wt% Pd and 5-wt% ceria, exhibiting maxima of 500 and 520 mW cm^{-2}, respectively. The open-circuit impedance data corresponding to these *V-i* curves are shown in **Figure 8*b***. For each of the cells, the ohmic losses varied between 0.30 and 0.38 Ω cm^2, in reasonable agreement with the expected ohmic loss for a 60-μm YSZ electrolyte, 0.32 Ω cm^2. This demonstrates that the LSCM-containing electrodes are electronically conductive. The big differences in the impedance spectra are associated with nonohmic losses. The electrode losses in the cell containing Pd are clearly much lower than those in the cell with only ceria, which in turn are much lower than those in the cell without added catalyst.

Interactions between the catalytic components and the electronically conductive ceramics do not appear to be critical for promoting electrode performance. Using LSCM for conductivity, performance enhancements similar to those observed with Pd were found following the addition of Pt, Rh, and Ni (74, 75). In all these cases, the amount of added metal (0.5 to 1 wt%) was negligible

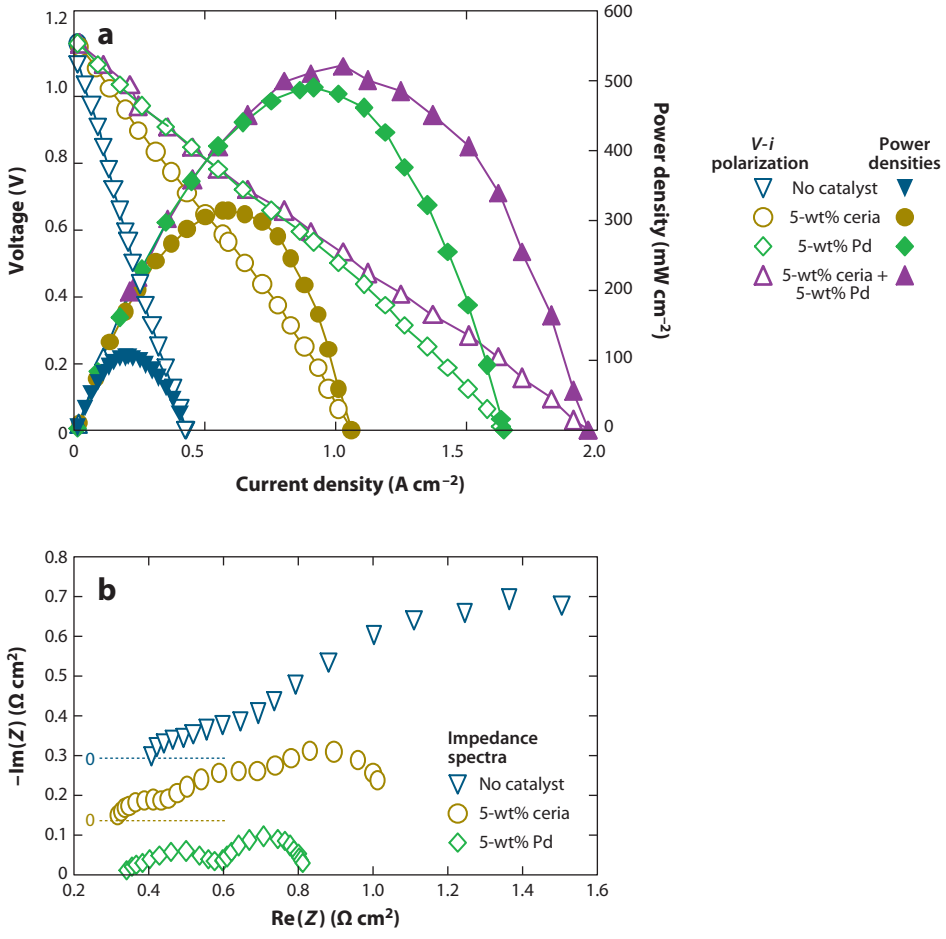

Figure 8

(*a*) *V-i* polarization curves in humidified H_2 (3% H_2O) at 973 K for cells containing anodes with 45 wt% $La_{0.8}Sr_{0.2}Cr_{0.5}Mn_{0.5}O_3$ (LSCM) in yttria-stabilized zirconia (YSZ), using various catalysts: (▽) no catalyst, (○) 5-wt% ceria, (◇) 0.5-wt% Pd, and (△) 5-wt% ceria and 0.5-wt% Pd. The filled symbols indicate the power densities. (*b*) Corresponding impedance spectra measured at open-circuit voltage for the cells with (▽) no catalyst, (○) 5-wt% ceria, and (◇) 0.5-wt% Pd. Only the high-frequency portion of the impedance curve of the cell without a catalyst is shown. Reproduced with permission from Reference 75, copyright © 2009, The Electrochemical Society.

compared with that which would be required to provide electronic conductivity, demonstrating that these metals were primarily catalytic. Furthermore, replacing infiltrated LSCM with other electronically conductive oxides, such as LST or ceria, gave almost identical results to those obtained with LSCM (76, 77). With all three oxides, the addition of a transition-metal catalyst greatly reduced the electrode impedance.

Kobsiriphat et al. (78) provides additional confirmation of the independence of the conductivity and catalytic functions within the SOFC anode in work on electrodes prepared by conventional screen-printing methods. In this study, Ru and Ni were incorporated into the electronically conductive perovskite, $La_{0.8}Sr_{0.2}CrO_3$. Under the strongly reducing conditions of the anode during cell operation, the transition metals were extruded from the oxide and formed small metal particles

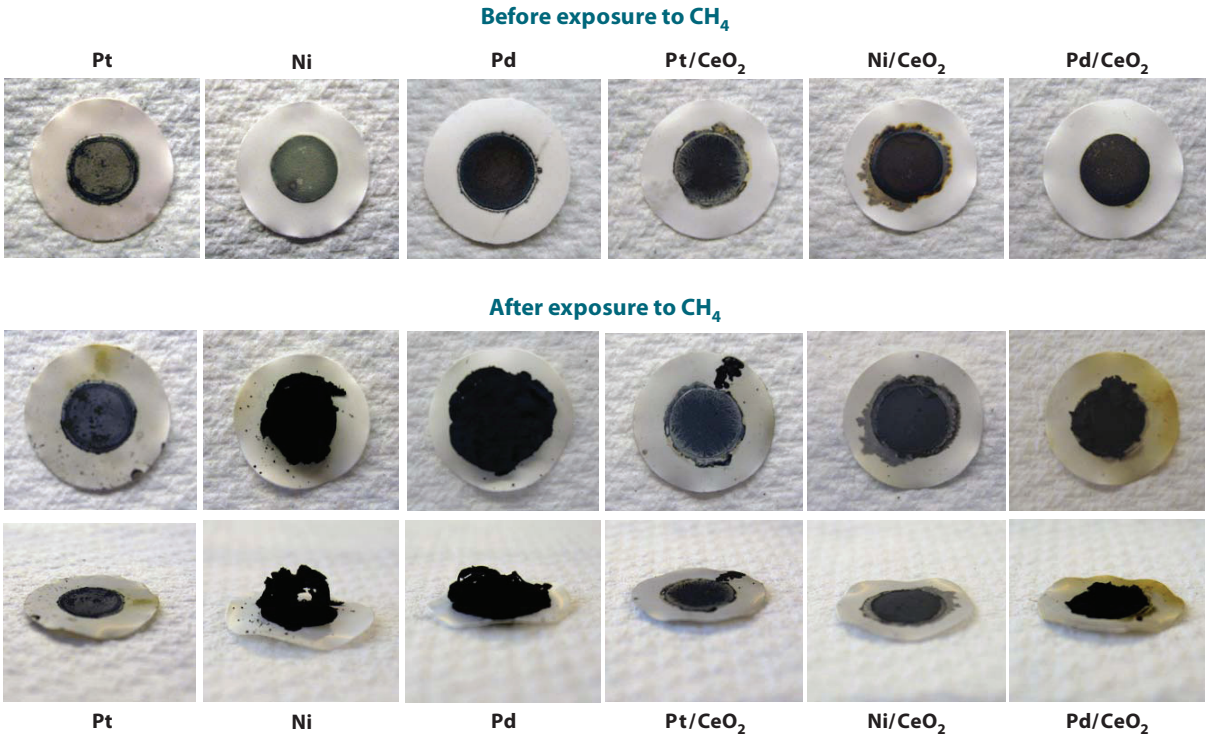

Figure 9

Photographs of $La_{0.8}Sr_{0.2}Cr_{0.5}Mn_{0.5}O_3$-yttria-stabilized zirconia (LSCM-YSZ) electrodes infiltrated with different catalysts. The upper set of images shows freshly reduced anodes, and the lower set of images was obtained after exposure to CH_4 at 973 K for 24 h. From Reference 74.

on the electrode surface. The electrode performance improved dramatically over time as the metal particles formed, which demonstrates the importance of the presence of a catalyst in the electrode. Although the long-term stability of the electrodes was not tested, it seems likely that interactions between the metal particles and the perovskite could help stabilize metal dispersion in a manner similar to that observed for Pd with $LaFeO_3$ supports (79).

The separation of conduction and catalytic properties as well as the ability to choose different catalytic metals have important implications for operating SOFCs on hydrocarbon fuels. In a study of infiltrated electrodes made with LSCM and 0.5-wt% Pt, Pd, or Ni, electrodes containing Pt were reasonably stable in CH_4 for at least 24 h, but carbon deposits with granular and filamentous morphologies were found on electrodes containing 0.5-wt% Pd or Ni (74). Carbon deposition on both Pd and Ni was greatly suppressed by the addition of 10-wt% ceria as a cocatalyst. These results are shown in the photographs in **Figure 9**.

ROLE OF CATALYSIS IN AIR ELECTRODES

In conventional, Ni-YSZ anode-supported SOFCs, the largest impedance is usually associated with the cathode. However, despite an extensive body of research, there is still no clear picture of what limits the performance of air electrodes and what the detailed mechanism is for the half-cell reaction in Equation 2. This section outlines some basic ideas about what we believe limits the performance of air electrodes. For a more complete review, the reader is referred elsewhere (8).

The requirement of electronic conductivity in a high-temperature, oxidizing environment can be met only by precious metals and conducting oxides; economics makes precious metals impractical. The most commonly used conductive oxides are doped perovskites; the prototypical material is LSM, with a typical composition of LSM being $La_{0.8}Sr_{0.2}MnO_{3-\delta}$. Compared with the situation with ceramic fuel electrodes, stable conductivity is easier to achieve with oxides in air because conductivity in oxides depends on the oxidation state (e.g., δ), which in turn depends on the $P(O_2)$. At the air electrode, the $P(O_2)$ is fixed near 0.21 atm, whereas the oxygen fugacity on the fuel side can vary by many orders of magnitude depending on the H_2:H_2O ratio and the temperature.

Most of the structural issues regarding TPB sites and the need for a good electrode-electrolyte interface, which were discussed earlier for fuel electrodes, apply equally well to air electrodes. The one major difference with air electrodes is that the best conductive oxides have MIEC, which widens the TPB region. Because the ionic conductivities of these materials are significantly less than that of YSZ, the best electrodes are still composites of the electronically conductive oxide and an electrolyte material, such as YSZ or doped ceria (8). Even though perovskites that exhibit lower impedances than LSM at low temperatures exist, LSM-based electrodes remain the standard materials in SOFC cathodes that utilize YSZ electrolytes because LSM is relatively resistant to reaction with YSZ at the sintering temperatures required for preparation of SOFC electrodes (14). When using other perovskite-based cathodes, it is usually necessary to introduce a barrier layer (e.g., doped ceria) between the perovskite and the YSZ to prevent these solid-state reactions (80, 81).

To understand the processes that occur at the electrochemically active region of an SOFC cathode (the region extending ~10 μm into the electrode), it is useful to consider the schematic shown in **Figure 10**. This diagram shows idealized YSZ channels that extend from the electrolyte into the electrode and are covered by a dense film of an MIEC perovskite. This structure is similar to that observed for electrodes prepared by infiltration of perovskites into a porous YSZ scaffold

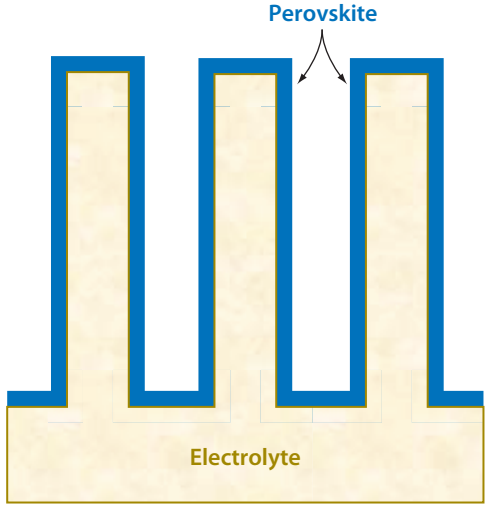

Figure 10

Schematic of the electrode structure used in the model described in the text. The schematic shows the region approximately in contact with the electrolyte and extending 10 μm into the electrode. This region is viewed as consisting of yttria-stabilized zirconia (YSZ) fins that are coated with a dense mixed ionic and electronic conductivity (MIEC) perovskite film.

after calcination to 1,373 K (82). Although calcination of perovskite-YSZ composites at lower temperatures results in the perovskite layer being particulate in nature and yields better electrode performance, the performance following this higher temperature treatment is reasonable for Sr-doped $LaFeO_3$ (LSF) in YSZ. Thus, the understanding we obtain from this model is likely valid for all composite electrodes. For this structure, the overall cathode reaction will involve gas-phase diffusion of O_2 into the composite, electrochemical oxidation of the perovskite surface, diffusion of the oxygen ions through the perovskite film, and transport of the ions down the YSZ fins, all of which take place in series.

Except for cells operating at extremely high current densities, gas-phase diffusion is fast, and concentration gradients in the gas phase can be ignored safely (83). Regarding diffusion of ions through the MIEC perovskite film, models have shown that the electrode impedance will scale with $\sigma_i^{-1/2}$, where σ_i is the ionic conductivity (23). The step that catalytic activity can affect is oxidation of the perovskite surface. If oxidation is fast, the surface will be in equilibrium with the gas phase, and δ can be determined from thermodynamic data, which are available for perovskites such as LSM and LSF (84, 85). The more interesting scenario occurs when the oxidation reaction is not fast compared with the diffusion rate. This is most often modeled using the Butler-Volmer equation, but, as discussed earlier, the applicability of this equation to SOFC electrodes is questionable. Assuming that oxygen vacancies in the perovskite do not interact, we suggest that the reaction of the oxygen vacancies with gas-phase oxygen can be treated using collision theory, with the effective reactive sticking coefficient being proportional to δ, according to Equation 8 (24):

$$S = S_0 \frac{\delta - \delta_0}{3 - \delta_0}. \qquad 8.$$

In this equation, S_0 is the probability that a molecule striking a vacancy will adsorb, and δ_0 is the equilibrium value for δ at 0.21 atm. $\delta/3$ is the fraction of oxygen-lattice sites that are vacant, and δ_0 is included in the final expression to allow for desorption of O_2 at 0.21 atm in the absence of electrode polarization. For dissociative adsorption, it would be better to assume that the adsorption rate is proportional to $(\delta/3)^2$, but we treat adsorption as linear for simplicity. If the perovskite has a high ionic conductivity, the surface will be in equilibrium with the $P(O_2)$ corresponding to the electrode overpotential, and δ will deviate from its equilibrium value at 0.21 atm.

Because the addition of a catalyst could affect only S_0, it is useful to estimate the values of S_0 that would be required to achieve reasonable electrode impedances. Using data for $La_{0.6}Sr_{0.4}FeO_3$ at 1,073 K and an overpotential of 0.2 V (85), the values for δ and δ_0 are 0.1 and 0.03, respectively. Assuming that the specific surface area of the electrode is 1 $m^2\ cm^{-3}$ and that its electrochemically active region is 10 μm thick, the calculated current density is $1{,}000 \cdot S_0$ A cm^{-2}. In other words, the impedance of the electrode would be $2 \times 10^{-4}\ S_0^{-1}\ \Omega\ cm^2$. Because a typical electrode impedance for an unmodified LSF-YSZ electrode would be $\sim 0.1\ \Omega \cdot cm^2$, S_0 would need to be approximately 10^{-3}, a reasonably high value for oxidation of a reduced oxide. The important point here is that it may not be possible to increase this value significantly by using a catalyst.

There has been a considerable effort aimed at improving the performance of perovskite-based air electrodes by adding catalytic components, but this approach has achieved only mixed success. Although Uchida and coworkers (86) reported that addition of Pt significantly enhanced the electrochemical performance of LSM-YSZ composites and Erning et al. (87) reported similar enhancements through the addition of Pd, Haanappel and coworkers (88) reported that neither Pd nor Pt had any effect on the performance of LSM cathodes. Discrepancies also exist for claims about the effect of infiltrated cobalt oxide. For example, Yamahara et al. (89, 90) reported significant improvements in cathode performance following the addition of small Co_3O_4 nanoparticles,

whereas Huang et al. (91) claimed that the incorporation of CoO_x had no effect on LSM-YSZ cathode impedances.

In an effort to determine the origin of these discrepancies, we recently reexamined the influence of various promoters on the performance of LSF-YSZ and LSM-YSZ electrodes (27). Because the structure of the perovskite-YSZ composites has such an important influence on electrode performance, we prepared the composite electrodes by infiltration of the metal salts to make the LSF or LSM, then calcined the final structures to 1,123 or 1,373 K to produce either particulate or film-like perovskites within the YSZ scaffold. The addition of dopants had little influence on the 1,123 K composite electrodes, but all dopants tested improved the performance of the 1,373 K composites. With 1,373 K, LSF-YSZ electrodes, the open-circuit impedances decreased dramatically following the addition of 10-wt% YSZ, 0.5-wt% Pd, 10-wt% $Ce_{0.8}Sm_{0.2}O_{1.9}$ (SDC), 10-wt% CaO, or 10-wt% K_2O. Similarly, the 1,373 K, LSM-YSZ electrodes were enhanced by the addition of 10-wt% CeO_2, 1-wt% Pd, or 10-wt% YSZ. Because the improved performance was close to that of the corresponding LSF-YSZ and LSM-YSZ electrodes that had been calcined to only 1,123 K and because the enhancements were lost following a second calcination to 1,373 K, it was concluded that the improved performance was related to structural changes in the electrode (i.e., increased specific surface area) rather than to improved catalytic properties or ionic conductivity.

SUMMARY AND FUTURE ISSUES

In this review we have highlighted the roles that catalysis plays in determining the performance of both anodes and cathodes in SOFCs and SOEs. As noted throughout the review, the high temperatures and harsh environments to which these electrodes are exposed during synthesis and operation constrains both the choice of catalytic materials and the methods by which they can be synthesized. Although catalysts and electrode structures that have high activity for oxygen reduction and for the oxidation of a range of fuels, including H_2 and hydrocarbons, have been identified, the need to increase both their stability under operating conditions and their activity to allow operation at lower temperatures are major issues that need to be addressed and are the focus of much of the research in this area. Mechanistic understanding of the catalytic reactions in SOFC and SOE electrodes also lags far behind that of more traditional heterogeneously catalyzed reactions and is an area that we believe needs further attention.

DISCLOSURE STATEMENT

The authors are not aware of any affiliations, memberships, funding, or financial holdings that might be perceived as affecting the objectivity of this review.

ACKNOWLEDGMENTS

We express our gratitude to the U.S. Department of Energy's Hydrogen Fuel Initiative (grant DE-FG02–05ER15721).

LITERATURE CITED

1. McIntosh S, Gorte RJ. 2004. Direct hydrocarbon solid oxide fuel cells. *Chem. Rev.* 104:4845–65
2. Bidrawn F, Kim G, Corre G, Irvine JTS, Vohs JM, Gorte RJ. 2008. Efficient reduction of CO_2 in a solid oxide electrolyzer. *Electrochem. Solid State Lett.* 11:B167–70

3. Jensen SH, Larsen PH, Mogensen M. 2007. Hydrogen and synthetic fuel production from renewable energy sources. *Int. J. Hydrogen Energy* 32:3253–57
4. Ormerod RM. 2003. Solid oxide fuel cells. *Chem. Soc. Rev.* 32:17–28
5. Steele BCH, Heinzel A. 2001. Materials for fuel-cell technologies. *Nature* 414:345–52
6. Zhu WZ, Deevi SC. 2003. A review on the status of anode materials for solid oxide fuel cells. *Mater. Sci. Eng. A* 362:228–39
7. Atkinson A, Barnett S, Gorte RJ, Irvine JTS, McEvoy AJ, et al. 2004. Advanced anodes for high-temperature fuel cells. *Nat. Mater.* 3:17–27
8. Adler SB. 2004. Factors governing oxygen reduction in solid oxide fuel cell cathodes. *Chem. Rev.* 104:4791–843
9. Boder M, Dittmeyer R. 2006. Catalytic modification of conventional SOFC anodes with a view to reducing their activity for direct internal reforming of natural gas. *J. Power Source* 155:13–22
10. Singhal S, Kendall K, eds. 2003. *High Temperature Solid Oxide Fuel Cells: Fundamentals, Design, and Applications*. Oxford: Elsevier
11. Tanner CW, Fung KZ, Virkar AV. 1997. The effect of porous composite electrode structure on solid oxide fuel cell performance. 1. Theoretical analysis. *J. Electrochem. Soc.* 144:21–30
12. Ullmann H, Trofimenko N, Tietz F, Stover D, Ahmad-Khanlou A. 2000. Correlation between thermal expansion and oxide ion transport in mixed conducting perovskite-type oxides for SOFC cathodes. *Solid State Ionics* 138:79–90
13. Fukunaga H, Ishino M, Yamada K. 2007. Effective thickness of Ni-Sm-doped ceria cermet anode for solid oxide fuel cell. *Electrochem. Solid State Lett.* 10:B16–18
14. Minh NQ. 1993. Ceramic fuel-cells. *J. Am. Ceramic Soc.* 76:563–88
15. Dees DW, Claar TD, Easler TE, Fee DC, Mrazek FC. 1987. Conductivity of porous Ni/ZrO_2-Y_2O_3 cermets. *J. Electrochem. Soc.* 134:2141–46
16. Haanappel VAC, Mertens J, Mai A. 2006. Performance improvement of $(La,Sr)MnO_3$ and $(La,Sr)_x(Co,Fe)O_3$-type anode-supported SOFCs. *J. Fuel Cell Sci. Technol.* 3:263–70
17. Zhao F, Virkar AV. 2005. Dependence of polarization in anode-supported solid oxide fuel cells on various cell parameters. *J. Power Sources* 141:79–95
18. Paunovic M, Schlesinger M. 2006. *Fundamentals of Electrochemical Deposition*. New York: Wiley
19. O'Brien JE, Stoots CM, Herring JS, Lessing PA, Hartvigsen JJ, Elangovan S. 2005. Performance measurements of solid-oxide electrolysis cells for hydrogen production. *J. Fuel Cell Sci. Technol.* 2:156–63
20. Wang WS, Huang YY, Jung SW, Vohs JM, Gorte RJ. 2006. A comparison of LSM, LSF, and LSCo for solid oxide electrolyzer anodes. *J. Electrochem. Soc.* 153:A2066–70
21. Kim G, Corre G, Irvine JTS, Vohs JM, Gorte RJ. 2008. Engineering composite oxide SOFC anodes for efficient oxidation of methane. *Electrochem. Solid State Lett.* 11:B16–19
22. McIntosh S, Vohs JM, Gorte RJ. 2003. Impedance spectroscopy for the characterization of Cu-Ceria-YSZ anodes for SOFCs. *J. Electrochem. Soc.* 150:A1305–12
23. Adler SB, Lane JA, Steele BCH. 1996. Electrode kinetics of porous mixed-conducting oxygen electrodes. *J. Electrochem. Soc.* 143:3554–64
24. Bidrawn B, Kungas R, Vohs JM, Gorte RJ. 2011. Modeling impedance response of SOFC cathodes prepared by infiltration. *J. Electrochem. Soc.* 158:B514–25
25. McIntosh S, Adler SB, Vohs JM, Gorte RJ. 2004. Effect of polarization on and implications for characterization of LSM-YSZ composite cathodes. *Electrochem. Solid State Lett.* 7:A111–14
26. Huang YY, Vohs JM, Gorte RJ. 2005. Characterization of LSM-YSZ composites prepared by impregnation methods. *J. Electrochem. Soc.* 152:A1347–53
27. Bidrawn F, Kim G, Aramrueang N, Vohs JM, Gorte RJ. 2010. Dopants to enhance SOFC cathodes based on Sr-doped $LaFeO_3$ and $LaMnO_3$. *J. Power Sources* 195:720–28
28. Woo LY, Glass RS, Gorte RJ, Orme CA, Nelson AJ. 2009. Dynamic changes in LSM nanoparticles on YSZ: a model system for non-stationary SOFC cathode behavior. *J. Electrochem. Soc.* 156:B602–8
29. Vayenas CG, Bebelis S, Ladas S. 1990. Dependence of catalytic rates on catalyst work function. *Nature* 343:625–27
30. Ladas S, Kennou S, Bebelis S, Vayenas CG. 1993. Origin of non-faradaic electrochemical modification of catalytic activity. *J. Phys. Chem.* 97:8845–48

31. Toghan A, Rosken LM, Imbihl R. 2010. The electrochemical promotion of ethylene oxidation at a Pt/YSZ catalyst. *ChemPhysChem* 11:1452–59
32. Marina OA, Sobyanin VA, Belyaev VD, Parmon VN. 1993. The effect of electrochemical pumping of oxygen on catalytic behavior of metal-electrodes in methane oxidation. *Stud. Surf. Sci. Catal.* 77:337–40
33. Koutsodontis C, Katsaounis A, Figueroa JC, Cavalca C, Pereira C, Vayenas CG. 2006. The effect of catalyst film thickness on the electrochemical promotion of ethylene oxidation on Pt. *Topics Catal.* 39:97–100
34. Steininger H, Ibach H, Lehwald S. 1982. Surface reactions of ethylene and oxygen on Pt(111). *Surf. Sci.* 117:685–98
35. Bunluesin T, Gorte RJ, Graham GW. 1997. CO oxidation for the characterization of reducibility in oxygen storage components of three-way automotive catalysts. *Appl. Catalysis B* 14:105–15
36. deSouza S, Visco SJ, DeJonghe LC. 1997. Reduced-temperature solid oxide fuel cell based on YSZ thin-film electrolyte. *J. Electrochem. Soc.* 144:L35–37
37. Foger K, Ahmed K. 2005. Catalysis in high-temperature fuel cells. *J. Phys. Chem. B* 109:2149–54
38. Herbstritt D, Weber A, Ivers-Tiffee E. 2001. Modelling and DC-polarisation of a three dimensional electrode/electrolyte interface. *J. Eur. Ceram. Soc.* 21:1813–16
39. Kim JW, Virkar AV, Fung KZ, Mehta K, Singhal SC. 1999. Polarization effects in intermediate temperature, anode-supported solid oxide fuel cells. *J. Electrochem. Soc.* 146:69–78
40. Chun CM, Bhargava G, Ramanarayanan TA. 2007. Metal dusting corrosion of nickel-based alloys. *J. Electrochem. Soc.* 154:C231–40
41. He HP, Hill JM. 2007. Carbon deposition on Ni/YSZ composites exposed to humidified methane. *Appl. Catal. A* 317:284–92
42. Cimenti M, Hill JM. 2009. Direct utilization of liquid fuels in SOFC for portable applications: challenges for the selection of alternative anodes. *Energies* 2:377–410
43. Ebbesen SD, Mogensen M. 2009. Electrolysis of carbon dioxide in solid oxide electrolysis cells. *J. Power Sour.* 193:349–58
44. Busawon AN, Sarantaridis D, Atkinson A. 2008. Ni infiltration as a possible solution to the redox problem of SOFC anodes. *Electrochem. Solid State Lett.* 11:B186–89
45. Kurokawa H, Sholklapper TZ, Jacobson CP, De Jonghe LC, Visco SJ. 2007. Ceria nanocoating for sulfur tolerant Ni-based anodes of solid oxide fuel cells. *Electrochem. Solid State Lett.* 10:B135–38
46. Matsuzaki Y, Yasuda I. 2000. The poisoning effect of sulfur-containing impurity gas on a SOFC anode: Part I. Dependence on temperature, time, and impurity concentration. *Solid State Ionics* 132:261–69
47. Gong MY, Liu XB, Trembly J, Johnson C. 2007. Sulfur-tolerant anode materials for solid oxide fuel cell application. *J. Power Sour.* 168:289–98
48. Zhan ZL, Barnett SA. 2005. An octane-fueled solid oxide fuel cell. *Science* 308:844–47
49. Pillai MR, Kim I, Bierschenk DM, Barnett SA. 2008. Fuel-flexible operation of a solid oxide fuel cell with $Sr_{0.8}La_{0.2}TiO_3$ support. *J. Power Sour.* 185:1086–93
50. Kim H, Lu C, Worrell WL, Vohs JM, Gorte RJ. 2002. Cu-Ni cermet anodes for direct oxidation of methane in solid-oxide fuel cells. *J. Electrochem. Soc.* 149:A247–50
51. Jung S, Gross MD, Gorte RJ, Vohs JM. 2006. Electrodeposition of Cu into a highly porous Ni/YSZ cermet. *J. Electrochem. Soc.* 153:A1539–43
52. Nikolla E, Schwank J, Linic S. 2009. Direct electrochemical oxidation of hydrocarbon fuels on SOFCs: improved carbon tolerance of Ni alloy anodes. *J. Electrochem. Soc.* 156:B1312–16
53. Nikolla E, Holewinski A, Schwank J, Linic S. 2006. Controlling carbon surface chemistry by alloying: carbon tolerant reforming catalyst. *J. Am. Chem. Soc.* 128:11354–55
54. Nikolla E, Schwank JW, Linic S. 2008. Hydrocarbon steam reforming on Ni alloys at solid oxide fuel cell operating conditions. *Catal. Today* 136:243–48
55. Kan H, Lee H. 2010. Sn-doped Ni/YSZ anode catalysts with enhanced carbon deposition resistance for an intermediate temperature SOFC. *Appl. Catalysis B* 97:108–14
56. Kurokawa H, Yang LM, Jacobson CP, De Jonghe LC, Visco SJ. 2007. Y-doped $SrTiO_3$ based sulfur tolerant anode for solid oxide fuel cells. *J. Power Sour.* 164:510–18
57. Tao SW, Irvine JTS. 2004. Discovery and characterization of novel oxide anodes for solid oxide fuel cells. *Chem. Record* 4:83–95

58. Fu QX, Tietz F. 2008. Ceramic-based anode materials for improved redox cycling of solid oxide fuel cells. *Fuel Cells* 8:283–93
59. van den Bossche M, Matthews R, Lichtenberger A, McIntosh S. 2010. Insights into the fuel oxidation mechanism of $La_{0.75}Sr_{0.25}Cr_{0.5}Mn_{0.5}O_{3-\delta}$ SOFC anodes. *J. Electrochem. Soc.* 157:B392–99
60. Lee SI, Vohs JM, Gorte RJ. 2004. A study of SOFC anodes based on Cu-Ni and Cu-Co bimetallics in CeO_2-YSZ. *J. Electrochem. Soc.* 151:A1319–23
61. Park S, Gorte RJ, Vohs JM. 2001. Tape cast solid oxide fuel cells for the direct oxidation of hydrocarbons. *J. Electrochem. Soc.* 148:A443–47
62. Ahn K, Jung S, Vohs JM, Gorte RJ. 2007. A support layer for solid oxide fuel cells. *Ceram. Int.* 33:1065–70
63. Gorte RJ, Park S, Vohs JM, Wang CH. 2000. Anodes for direct oxidation of dry hydrocarbons in a solid-oxide fuel cell. *Adv. Mater.* 12:1465–69
64. Vohs JM, Gorte RJ. 2009. High-performance SOFC cathodes prepared by infiltration. *Adv. Mater.* 21:943–56
65. Zhu X, Lu Z, Wei B, Zhang Y, Huang X, Su W. 2010. Impregnated $La_{0.75}Sr_{0.25}Cr_{0.5}Fe_{0.5}O_{3-d}$-based anodes operating on H_2, CH_4, and C_2H_5OH fuels. *Electrochem. Solid State Lett.* 13:B91–94
66. Craciun R, Park S, Gorte RJ, Vohs JM, Wang C, Worrell WL. 1999. A novel method for preparing anode cermets for solid oxide fuel cells. *J. Electrochem. Soc.* 146:4019–22
67. Park S, Craciun R, Vohs JM, Gorte RJ. 1999. Direct oxidation of hydrocarbons in a solid oxide fuel cell: I. Methane oxidation. *J. Electrochem. Soc.* 146:3603–5
68. Park SD, Vohs JM, Gorte RJ. 2000. Direct oxidation of hydrocarbons in a solid-oxide fuel cell. *Nature* 404:265–67
69. Lu C, Worrell WL, Vohs JM, Gorte RJ. 2003. A comparison of Cu-ceria-SDC and Au-ceria-SDC composites for SOFC anodes. *J. Electrochem. Soc.* 150:A1357–59
70. McIntosh S, Vohs JM, Gorte RJ. 2002. An examination of lanthanide additives on the performance of Cu-YSZ cermet anodes. *Electrochim. Acta* 47:3815–21
71. Jung SW, Lu C, He HP, Ahn KY, Gorte RJ, Vohs JM. 2006. Influence of composition and Cu impregnation method on the performance of Cu/CeO_2/YSZ SOFC anodes. *J. Power Sour.* 154:42–50
72. Gross MD, Vohs JM, Gorte RJ. 2007. A study of thermal stability and methane tolerance of Cu-based SOFC anodes with electrodeposited Co. *Electrochim. Acta* 52:1951–57
73. Lee SI, Ahn K, Vohs JM, Gorte RJ. 2005. Cu-Co bimetallic anodes for direct utilization of methane in SOFCs. *Electrochem. Solid State Lett.* 8:A48–51
74. Kim JS, Nair VV, Vohs JM, Gorte RJ. 2010. A study of the methane tolerance of LSCM-YSZ composite anodes with Pt, Ni, Pd and ceria catalysts. *Scripta Mater.* doi:10.1016/j.scriptamat.2010.06016. In press
75. Kim G, Lee S, Shin JY, Corre G, Irvine JTS, et al. 2009. Investigation of the structural and catalytic requirements for high-performance SOFC anodes formed by infiltration of LSCM. *Electrochem. Solid State Lett.* 12:B48–52
76. Lee S, Kim G, Vohs JM, Gorte RJ. 2008. SOFC anodes based on infiltration of $La_{0.3}Sr_{0.7}TiO_3$. *J. Electrochem. Soc.* 155:B1179–83
77. Kim G, Vohs JM, Gorte RJ. 2008. Enhanced reducibility of ceria-YSZ composites in solid oxide electrodes. *J. Mater. Chem.* 18:2386–90
78. Kobsiriphat W, Madsen BD, Wang Y, Shah M, Marks LD, Barnett SA. 2010. Nickel- and ruthenium-doped lanthanum chromite anodes: effects of nanoscale metal precipitation on solid oxide fuel cell performance. *J. Electrochem. Soc.* 157:B279–84
79. Nishihata Y, Mizuki J, Tanaka H, Uenishi M, Kimura M. 2005. Self-regeneration of palladium-perovskite catalysts in modem automobiles. *J. Phys. Chem. Solids* 66:274–82
80. Shiono M, Kobayashi K, Nguyen TL, Hosoda K, Kato T, et al. 2004. Effect of CeO_2 interlayer on ZrO_2 electrolyte/La(Sr)CoO_3 cathode for low-temperature SOFCs. *Solid State Ionics* 170:1–7
81. Rossignol C, Ralph JM, Bae JM, Vaughey JT. 2004. $Ln_{1-x}Sr_xCoO_3$ (Ln = Gd, Pr) as a cathode for intermediate-temperature solid oxide fuel cells. *Solid State Ionics* 175:59–61
82. Wang WS, Gross MD, Vohs JM, Gorte RJ. 2007. The stability of LSF-YSZ electrodes prepared by infiltration. *J. Electrochem. Soc.* 154:B439–45
83. Costa-Nunes O, Vohs JM, Gorte RJ. 2003. A study of direct-conversion SOFC with *n*-butane at higher fuel utilization. *J. Electrochem. Soc.* 150:A858–63

84. Mizusaki J, Mori N, Takai H, Yonemura Y, Minamiue H, et al. 2000. Oxygen nonstoichiometry and defect equilibrium in the perovskite-type oxides $La_{1-x}Sr_xMnO_{3-\delta}$. *Solid State Ionics* 129:163–77
85. Mosleh M, Sogaard M, Hendriksen PV. 2009. Kinetics and mechanisms of oxygen surface exchange on $La_{0.6}Sr_{0.4}FeO_{3-\delta}$ thin films. *J. Electrochem. Soc.* 156:B441–57
86. Uchida H, Yoshida M, Watanabe M. 1999. Effect of ionic conductivity of zirconia electrolytes on the polarization behavior of various cathodes in solid oxide fuel cells. *J. Electrochem. Soc.* 146:1–7
87. Erning JW, Hauber T, Stimming U, Wippermann K. 1996. Catalysis of the electrochemical processes on solid oxide fuel cell cathodes. *J. Power Sour.* 61:205–11
88. Haanappel VAC, Rutenbeck D, Mai A, Uhlenbruck S, Sebold D, et al. 2004. The influence of noble-metal-containing cathodes on the electrochemical performance of anode-supported SOFCs. *J. Power Sour.* 130:119–28
89. Yamahara K, Jacobson CP, Visco SJ, De Jonghe LC. 2005. Catalyst-infiltrated supporting cathode for thin-film SOFCs. *Solid State Ionics* 176:451–56
90. Yamahara K, Jacobson CP, Visco SJ, Zhang XF, de Jonghe LC. 2005. Thin film SOFCs with cobalt-infiltrated cathodes. *Solid State Ionics* 176:275–79
91. Huang YY, Vohs JM, Gorte RJ. 2006. An examination of LSM-LSCo mixtures for use in SOFC cathodes. *J. Electrochem. Soc.* 153:A951–55

Annual Review of Chemical and Biomolecular Engineering

Volume 2, 2011

Contents

My Contribution to Broadening the Base of Chemical Engineering
Roger W.H. Sargent 1

Catalysis for Solid Oxide Fuel Cells
R.J. Gorte and J.M. Vohs 9

CO_2 Capture from Dilute Gases as a Component of Modern Global Carbon Management
Christopher W. Jones 31

Engineering Antibodies for Cancer
Eric T. Boder and Wei Jiang 53

Silencing or Stimulation? siRNA Delivery and the Immune System
Kathryn A. Whitehead, James E. Dahlman, Robert S. Langer, and Daniel G. Anderson 77

Solubility of Gases and Liquids in Glassy Polymers
Maria Grazia De Angelis and Giulio C. Sarti 97

Deconstruction of Lignocellulosic Biomass to Fuels and Chemicals
Shishir P.S. Chundawat, Gregg T. Beckham, Michael E. Himmel, and Bruce E. Dale 121

Hydrophobicity of Proteins and Interfaces: Insights from Density Fluctuations
Sumanth N. Jamadagni, Rahul Godawat, and Shekhar Garde 147

Risk Taking and Effective R&D Management
William F. Banholzer and Laura J. Vosejpka 173

Novel Solvents for Sustainable Production of Specialty Chemicals
Ali Z. Fadhel, Pamela Pollet, Charles L. Liotta, and Charles A. Eckert 189

Metabolic Engineering for the Production of Natural Products
Lauren B. Pickens, Yi Tang, and Yit-Heng Chooi 211

Fundamentals and Applications of Gas Hydrates
Carolyn A. Koh, E. Dendy Sloan, Amadeu K. Sum, and David T. Wu 237

Crystal Polymorphism in Chemical Process Development
Alfred Y. Lee, Deniz Erdemir, and Allan S. Myerson 259

Delivery of Molecular and Nanoscale Medicine to Tumors: Transport Barriers and Strategies
Vikash P. Chauhan, Triantafyllos Stylianopoulos, Yves Boucher, and Rakesh K. Jain 281

Surface Reactions in Microelectronics Process Technology
Galit Levitin and Dennis W. Hess 299

Microfluidic Chemical Analysis Systems
Eric Livak-Dahl, Irene Sinn, and Mark Burns 325

Microsystem Technologies for Medical Applications
Michael J. Cima 355

Low–Dielectric Constant Insulators for Future Integrated Circuits and Packages
Paul A. Kohl 379

Tissue Engineering and Regenerative Medicine: History, Progress, and Challenges
François Berthiaume, Timothy J. Maguire, and Martin L. Yarmush 403

Intensified Reaction and Separation Systems
Andrzej Górak and Andrzej Stankiewicz 431

Quantum Mechanical Modeling of Catalytic Processes
Alexis T. Bell and Martin Head-Gordon 453

Progress and Prospects for Stem Cell Engineering
Randolph S. Ashton, Albert J. Keung, Joseph Peltier, and David V. Schaffer 479

Battery Technologies for Large-Scale Stationary Energy Storage
Grigorii L. Soloveichik 503

Coal and Biomass to Fuels and Power
Robert H. Williams, Guangjian Liu, Thomas G. Kreutz, and Eric D. Larson 529

Errata

An online log of corrections to *Annual Review of Chemical and Biomolecular Engineering* articles may be found at http://chembioeng.annualreviews.org/errata.shtml